POLITECNICO DI TORINO
Repository ISTITUZIONALE

Energy efficiency maximization in MIMO links aided by metasurfaces with global reflection constraints

Original
Energy efficiency maximization in MIMO links aided by metasurfaces with global reflection constraints / Tunal, I., Fotock, R.K., Zappone, A., Taricco, G., Alfano, G., Çrpan, H.A.. - In: EURASIP JOURNAL ON ADVANCES IN SIGNAL PROCESSING. - ISSN 1687-6172. - STAMPA. - 2025:1(2025). [10.1186/s13634-025-01233-8]

Availability:
This version is available at: 11583/3002095 since: 2025-09-13T20:16:43Z

Publisher:
Springer Nature

Published
DOI:10.1186/s13634-025-01233-8

Terms of use:

This article is made available under terms and conditions as specified in the corresponding bibliographic description in the repository

Publisher copyright

(Article begins on next page)

27 November 2026

Tunalı *et al.*
EURASIP Journal on Advances in Signal Processing (2025) 2025:29
https://doi.org/10.1186/s13634-025-01233-8

EURASIP Journal on Advances in Signal Processing

RESEARCH Open Access

Energy efficiency maximization in MIMO links aided by metasurfaces with global reflection constraints

Ayşegül Ilay Tunalı[1,2,4], Robert Kuku Fotock[3], Alessio Zappone[1,3*], Giorgio Taricco[1,2], Giuseppa Alfano[1,3] and Hakan Ali Çırpan[4]

*Correspondence:
alessio.zappone@unicas.it

[1] Consorzio Nazionale Interuniversitario per le Telecomunicazioni - CNIT, Parma, Italy
[2] Politecnico di Torino, Turin, Italy
[3] University of Cassino and Southern Lazio, Cassino, Italy
[4] Istanbul Technical University, Istanbul, Turkey

Abstract

This work develops two radio resource allocation algorithms to optimize the energy efficiency of a multiple-input multiple-output (MIMO) communication system where a metasurface is deployed near the transmit antenna array to create a reconfigurable holographic beamforming structure. The design involves jointly optimizing the transmit covariance matrix and the reflection coefficients of the reconfigurable holographic surface (RHS). Two methods are proposed for this joint optimization. In both approaches, the RHS matrix is optimized using sequential fractional programming. However, the transmit covariance matrix is optimized differently: the first method employs fractional programming, while the second method utilizes a search within a standard-compliant codebook. The two algorithms are compared, showing that the codebook-based method achieves performance with only a limited gap compared to the more complex sequential fractional programming algorithm. The analysis considers both a nearly-passive RHS and an active one equipped with analog amplifiers.

Keywords: Holographic beamforming, Reconfigurable holographic metasurfaces, Reconfigurable intelligent surfaces, Energy efficiency, Radio resource allocation

1 Introduction

The use of reconfigurable metasurfaces has emerged as a major candidate technology for future wireless 6G networks, due to their energy efficiency (EE) and the possibility to deploy a larger number of electromagnetic elements than with a traditional antenna array [1–4]. Increasing the EE of wireless networks is a major requirement of future 6G networks, because leading 5G technologies based on active antennas require a high energy consumption, which is not sustainable due to the rapid growth of mobile connectivity demands and rise of new services. In [5], it is argued that 5G technologies like massive multiple-input multiple-output (MIMO) provide much higher rate levels, but at the price of a power consumption that can be up to three times higher than legacy 4G technologies, mainly due to the large size of digital antenna arrays. In this context, metasurfaces allow for the possibility of reducing the number of antennas deployed at

Springer Open

© The Author(s) 2025. **Open Access** This article is licensed under a Creative Commons Attribution-NonCommercial-NoDerivatives 4.0 International License, which permits any non-commercial use, sharing, distribution and reproduction in any medium or format, as long as you give appropriate credit to the original author(s) and the source, provide a link to the Creative Commons licence, and indicate if you modified the licensed material. You do not have permission under this licence to share adapted material derived from this article or parts of it. The images or other third party material in this article are included in the article's Creative Commons licence, unless indicated otherwise in a credit line to the material. If material is not included in the article's Creative Commons licence and your intended use is not permitted by statutory regulation or exceeds the permitted use, you will need to obtain permission directly from the copyright holder. To view a copy of this licence, visit http://creativecommons.org/licenses/by-nc-nd/4.0/.

the transmitter and receiver, without sacrificing array gain thanks to the large number of surface elements. Moreover, metasurfaces can be either nearly-passive, i.e. no amplifier is equipped at the metasurface, and the only energy that is required for their operation is that needed to operate the hardware components that enable the reconfiguration of the reflecting elements, or active, i.e. analog amplifiers are equipped at the metasurface, to combat the so-called double or multiplicative fading effect [6, 7]. However, while active reconfigurable metasurfaces provide higher rate, their EE may be lower than that provided by nearly-passive metasurfaces, due to the additional energy consumption caused by the presence of the analog amplifiers [8].

1.1 Prior work

The majority of available works focus on metasurface-aided systems with multiple-antenna base stations (BSs), but single-antenna mobile terminals. This results in a system with array gain, but no multiplexing gain, thus severely limiting the rate and EE that can be achieved. Nevertheless, multiple-input single-output (MISO) channels are typically considered in metasurface-aided literature, because this scenario is more mathematically tractable than a full MIMO system. In the context of EE optimization, the vast majority of previous studies assumes the metasurfaces are deployed far from the transmit antennas [9, 10], and subsequent works along this line of research. In this context, metasurfaces are typically referred to as reconfigurable intelligent surfaces (RISs), and far-field propagation through the traditional plane wave model is assumed. In [11], the BS transmit power is minimized in a vehicular network aided by an omnidirectional RIS. In [12], sum-rate maximization and power consumption minimization are addressed in a RIS-aided network, through the allocation of the RIS reflection coefficients, and BS transmit powers. Different hardware architectures for active RISs are explored in [13], maximizing the system EE through the optimization of the RIS reflection coefficients and transmit beamforming. In [14], the EE of a multi-user RIS-aided MISO network is maximized by allocating the BS beamforming and the RIS reflection coefficients. In [15], a hybrid RIS is considered, which is equipped with both nearly-passive and active elements. The amount of passive and active elements to be used is optimized with the goal of maximizing the minimum EE of the mobile terminals, assuming a single-antenna BS. In [16], a satellite communication in the presence of an eavesdropper is considered, in which an active RIS with local reflection capabilities is used to boost the received power. In [8], the uplink of a MISO system is considered, and the EE is maximized with respect to the RIS reflection coefficients, the users transmit powers, and BS receive filters, and considering both passive and active metasurfaces. In [17], the secrecy EE of an RIS-aided network is maximized by deep reinforcement learning. In [18], alternating maximization and sequential programming are used to maximize the EE of a multi-user network with secrecy constraints enforced on the communication content. Similarly, in [19], sequential programming and alternating optimization are combined to optimize the minimum among the EEs of the mobile users in a multi-user network.

Besides their application as a way of controlling the propagation environment, more recently, the use of reconfigurable metasurfaces has been proposed also as an efficient way of implementing holographic beamforming [20, 21]. In this case, the metasurface is commonly referred to as a reconfigurable holographic surface (RHS). Compared to

active antenna arrays, RHSs have a lower energy expenditure [22] and can be equipped with a larger number of antenna elements [23–25]. RHSs are being considered an energy-efficient evolution of the massive MIMO technology [26]. In [27] a BS equipped with a switch-controlled RHS-aided beamforming architecture is considered, and the EE maximization problem is tackled via alternating optimization of the holographic beamformer, the digital beamformer, and the transmit power. A near-field channel model was proposed in [28], and the capacity limit of a point-to-point MIMO system with holographic beamforming is investigated.

In [29], the use of stacked intelligent metasurfaces (SIMs) has been explored for holographic beamforming. In this context, a MIMO system is considered, and the SIM is designed to establish a desired equivalent MIMO channel. In [30], RHSs are considered for THz-based networks, developing a model and analyzing the resulting performance. In [31], an electromagnetic framework for designing a holographic surface is developed. The performance and power consumption of the framework were compared to those of passive metasurfaces and MIMO digital antenna arrays. In [32], channel models for holographic MIMO communications are developed, and the system spectral efficiency is analyzed. In all papers on RHSs mentioned above, the RHS is wired to the radio frequency chains of the transceiver. On the other hand, fewer works consider holographic beamforming by RHSs that are not wired with the antenna feeders. In this configuration, the RHS is simply deployed in the vicinity of the transceiver to reflect/refract the signal transmitted by the digital antennas. The EE of this system is analyzed in [33], considering metasurfaces with local reflection capabilities. In [34], one RHS is placed in the near-field of the transmitter, and its size is optimized for EE maximization. A similar metasurface architecture is also considered in [35, 36], where it is referred to as reconfigurable intelligent BS. The use of an RHS has been considered also in networks aided by unmanned aerial vehicles (UAVs), as a way of aiding the communications and performing energy harvesting to power the UAV [37]. Wireless RHSs are also considered in [38], where the weighted sum-rate maximization problem is tackled in the downlink of a multi-user network in which a BS with a uniform linear array serves single-antenna users through multiple RHSs. All previous works did not consider EE optimization in systems with multiple antennas at both the transmitter and receiver. Indeed, only a few studies have focused on EE optimization in metasurface-aided MIMO systems, and the optimal EE in this scenario is still an open problem. In [39], upper- and lower-bounds on the EE of a MIMO link are optimized assuming a single-stream transmission. In [40], the trade-off between EE and spectral efficiency is studied, employing the weighted minimum mean squared error method to tackle the problem. In [41], the EE of a MIMO link employing simultaneous wireless information and power transfer (SWIPT) is considered. However, this work does not optimize the EE, which is defined as the ratio between rate and power consumption, addressing instead the simpler problem of minimizing the difference between rate and power. In [42], a MIMO network with finite block-length transmissions is considered, and the network EE is optimized through sequential fractional programming.

1.2 Contributions

Building on the context outlined above, this work presents the following contributions:

- We address the problem of EE maximization in a MIMO link, i.e. both the transmitter and the receiver have multiple antennas. In addition, a metasurface is deployed in the immediate vicinity of the transmit array, but is not wired to the transmitter. Although a single link is considered, the presence of multiple antennas at both ends of the communication makes the problem very challenging, due to the more complex expression of the EE that emerges. The model proposed is sufficiently general to encompass both far-field and near-field signal propagation, allowing to consider the deployment of the metasurface in the near-field of the BS antennas.
- In the considered setup, we develop a novel, provably convergent, optimization algorithm for EE maximization, based on a new reformulation of rank-one constraints coupled with sequential programming. Unlike other available optimization approaches for MIMO links with metasurfaces, the proposed approach limits the use of sequential optimization to a vector-valued function, rather than a matrix-valued function, thus reducing the computational complexity.
- In addition, we consider the optimization of the transmit covariance matrix by two approaches, one that employs fractional programming techniques, and another one that makes use of standard-compliant codebooks. The performance in the two cases is compared to assess the gap between practical, standard-compliant approaches and theoretical optimization techniques. Numerical results are provided to evaluate the performance of the proposed optimization methods.
- All points above are developed considering metasurfaces with global reflection constraints, which are more general than classical metasurfaces with local reflection constraints. Specifically, while local metasurface treat each reflecting element separately, enforcing that each local reflection coefficient has modulus not greater than one, the global reflection constraint enforces that the total power reflected by the complete metasurface is not greater than the total power that impinges on the metasurface.

2 System model

Let us consider a single-user MIMO link, in which a BS with N_T antennas communicates with a mobile terminal with N_R antennas, through a nearly-passive RHS equipped with N reflecting elements. Both transmit and receive antenna arrays, and RHS elements, are arranged in a rectangular pattern, with horizontal and vertical spacing $(\Delta_{h,t}, \Delta_{v,t})$ for the transmit antenna array, $(\Delta_{h,r}, \Delta_{v,r})$ for the receive antenna array, and (Δ_h, Δ_v) for the RHS. The RHS is deployed within the region defined by the Fraunhofer distance from the transmitter, and therefore it is within the near-field zone of the transmit antenna array. We recall that the Fraunhofer distance for a planar array is given by

$$r = \frac{2D^2}{\lambda}, \tag{1}$$

where λ is the wavelength of the transmit signal and D is the aperture of the antenna array, which, for a rectangular array is equal to the largest of the two dimensions.

2.1 Channel model

Let $\boldsymbol{H}$ and $\boldsymbol{G}$ denote the $N \times N_T$ and $N_R \times N$ channels between the BS and the RHS and between the RHS and the receiver. As for the channel matrix $\boldsymbol{H}$, since the RHS is in the near-field of the transmit array, its entries follow the (deterministic) spherical wave equation, i.e. the (n, m) element of $\boldsymbol{H}$, with $n = 1, \ldots, N$ and $m = 1, \ldots, N_T$, is expressed as

$$H(n,m) = \frac{\lambda}{4\pi}\sqrt{\alpha_{n,m}^{RHS}\alpha_{n,m}^{BS}}\frac{e^{-j(2\pi/\lambda)\|\boldsymbol{r}_n^{RHS}-\boldsymbol{r}_m^{BS}\|}}{\|\boldsymbol{r}_n^{RHS}-\boldsymbol{r}_m^{BS}\|}, \tag{2}$$

wherein $\boldsymbol{r}_n^{RHS}$ and $\boldsymbol{r}_m^{BS}$ are the vectors defining the 3D positions of the n-th RHS element and m-th BS antenna, $\alpha_{m,n}^{BS}$ denotes the transmit gain of the m-th transmit antenna toward the n-th RHS element and $\alpha_{m,n}^{RHS}$ denotes the receive gain of the n-th RHS element from the m-th transmit antenna. The gains $\alpha_{m,n}^{BS}$ and $\alpha_{m,n}^{RHS}$ are expressed as

$$\alpha_{n,m}^{BS} = \frac{4\pi}{\lambda^2}\Delta_{h,t}\Delta_{v,t}\rho_{n,m}^{BS} \tag{3}$$

$$\alpha_{n,m}^{RHS} = \frac{4\pi}{\lambda^2}\Delta_{h}\Delta_{v}\rho_{n,m}^{RHS}, \tag{4}$$

with $\rho_{n,m}^{BS}$ and $\rho_{n,m}^{RHS}$ the standard directivity factors of the BS antenna array and RHS, respectively [43, 44].

Instead, as for the channel matrix $\boldsymbol{G}$ between the RHS and the receiver, a traditional far field model holds, and in particular we consider that each entry of $\boldsymbol{G}$ is a realization of a Rice random variable with factor K, scaled by the path-loss coefficient

$$\mathrm{PL} = \mathrm{PL}_0\left(\frac{d}{d_0}\right)^{-\nu}, \tag{5}$$

where PL_0 is the path-loss at the reference distance d_0, d is the distance between the RHS and the receiver, and ν is the path-loss exponent.

1 ***Remark 1***

In the following, perfect channel state information (CSI) is assumed to be available for resource allocation purposes. As for the channel $\boldsymbol{H}$*, it follows the deterministic model described above, and so it is perfectly known since both the BS and the RHS are fixed devices. As for the channel* $\boldsymbol{G}$*, it is affected by random fading, and so it must be estimated. During the channel estimation phase, it is possible to set the RHS reflection matrix to the identity matrix, or to any other fixed matrix that simplifies the estimation process. Thus, recalling that* $\boldsymbol{H}$ *is deterministically known, the estimation of* $\boldsymbol{G}$ *reduces to the estimation of a conventional MIMO channel, which can be accomplished by traditional blind or pilot-based methods. We assume that the resulting estimation error is negligible at the*

design stage, which is realistic for scenarios in which the receiver has low-mobility, e.g. to indoor scenarios, or outdoor scenarios with pedestrian mobile users. Nevertheless, the performance analysis in Sect. 6 addresses the mismatch between the estimated channel and the true channel, showing that the algorithms proposed are robust against imperfect CSI at the transmitter.

2.2 Problem formulation

After defining the channel model, let us denote by $\boldsymbol{Q}$ the transmit covariance matrix, $\boldsymbol{\Gamma} = \text{diag}(\gamma_{1,1}, \ldots, \gamma_{N,N})$ the RHS matrix, $\boldsymbol{s}$ the $N_T \times 1$ vector of transmit symbols, with $\mathbb{E}[\boldsymbol{s}\boldsymbol{s}^H] = \boldsymbol{I}_{N_T}$, $\boldsymbol{n} \sim \mathcal{CN}(\boldsymbol{0}, \sigma^2\boldsymbol{I})$ the thermal noise at the receiver, B the communication bandwidth. Then, the signal that impinges on the RHS is given by

$$\boldsymbol{r} = \boldsymbol{H}\boldsymbol{Q}^{1/2}\boldsymbol{s}, \tag{6}$$

and so, after applying the reflection matrix $\boldsymbol{\Gamma}$, and propagation over the channel $\boldsymbol{G}$, the signal received at the final destination is given by

$$\boldsymbol{y} = \boldsymbol{G}\boldsymbol{\Gamma}\boldsymbol{H}\boldsymbol{Q}^{1/2}\boldsymbol{s} + \boldsymbol{n}, \tag{7}$$

wherein we have exploited the fact that the metasurface does not introduce any noise amplification, being a passive device. Moreover, let us denote by $\mu \geq 1$ the inverse of the transmit amplifier efficiency, and by P_c the total hardware power consumed in the system, which can be modeled as

$$P_c = NP_{c,n} + N_T P_{c,t} + N_R P_{c,r} + P_{c,0}, \tag{8}$$

wherein $P_{c,n}$ is the static power consumed by each metasurface element, $P_{c,t}$ is the static power consumed by each antenna of the transmit array, $P_{c,r}$ is the static power consumed by each antenna of the receive array, and $P_{c,0}$ is the static power consumed by all other circuitry in the system. Then, the total power consumption of the system is $P_t = \mu\text{tr}(\boldsymbol{Q}) + P_c$, and the system capacity and EE are given by

$$C = B\log_2\left|\boldsymbol{I} + \frac{1}{\sigma^2}\boldsymbol{G}\boldsymbol{\Gamma}\boldsymbol{H}\boldsymbol{Q}\boldsymbol{H}^H\boldsymbol{\Gamma}^H\boldsymbol{G}^H\right|, \text{ [bit/s]} \tag{9}$$

$$\text{EE} = \frac{C}{P_t} = B\frac{\log_2\left|\boldsymbol{I} + \frac{1}{\sigma^2}\boldsymbol{G}\boldsymbol{\Gamma}\boldsymbol{H}\boldsymbol{Q}\boldsymbol{H}^H\boldsymbol{\Gamma}^H\boldsymbol{G}^H\right|}{\mu\text{tr}(\boldsymbol{Q}) + P_c}, \text{ [bit/J]} \tag{10}$$

In this work, we consider a metasurface with global reflection constraints. As opposed to metasurface with local reflection constraints, in which each reflection coefficient is separately constrained to have modulus lower than one, in a metasurface with global reflection constraints, a single reflection constraint is enforced on all of the reflection coefficients, requiring that the reflection matrix $\boldsymbol{\Gamma}$ is such that $P_{out} \leq P_{in}$, wherein P_{out} is the power that departs from the metasurface and P_{in} is the power that impinges on the metasurface. These powers are given by

$$P_{in} = \mathbb{E}[\text{tr}(\boldsymbol{H}\boldsymbol{Q}^{1/2}\boldsymbol{s}\boldsymbol{s}^H\boldsymbol{Q}^{1/2}\boldsymbol{H}^H)] = \text{tr}(\boldsymbol{H}\boldsymbol{Q}\boldsymbol{H}^H) \tag{11}$$

$$P_{out} = \mathbb{E}[\mathrm{tr}(\boldsymbol{\Gamma H Q}^{1/2}\boldsymbol{s})(\boldsymbol{s}^H\boldsymbol{Q}^{1/2}\boldsymbol{H}^H\boldsymbol{\Gamma}^H)] = \mathrm{tr}(\boldsymbol{\Gamma H Q H}^H\boldsymbol{\Gamma}^H) \tag{12}$$

Thus, the global reflection constraint at the metasurface is formulated as

$$\mathrm{tr}(\boldsymbol{\Gamma H Q H}^H\boldsymbol{\Gamma}^H) \leq \mathrm{tr}(\boldsymbol{H Q H}^H). \tag{13}$$

Moreover, denoting by P_{max} the maximum transmit power at the BS, the problem of EE maximization with respect to the metasurface matrix and the transmit covariance matrix can be cast as

$$\max_{\boldsymbol{Q},\boldsymbol{\Gamma}} B\frac{\log_2\left|\boldsymbol{I} + \frac{1}{\sigma^2}\boldsymbol{G\Gamma H Q H}^H\boldsymbol{\Gamma}^H\boldsymbol{G}^H\right|}{\mu\mathrm{tr}(\boldsymbol{Q}) + P_c} \tag{14a}$$

$$\text{s.t. } \mathrm{tr}(\boldsymbol{\Gamma H Q H}^H\boldsymbol{\Gamma}^H) \leq \mathrm{tr}(\boldsymbol{H Q H}^H) \tag{14b}$$

$$\mathrm{tr}(\boldsymbol{Q}) \leq P_{max}\ ,\ \boldsymbol{Q} \succeq \boldsymbol{0} \tag{14c}$$

Problem (14) is a non-convex fractional program, which cannot be solved by simply applying convex optimization or fractional programming theory, due to the fact that the numerator of (14a) is not jointly concave in $(\boldsymbol{Q}, \boldsymbol{\Gamma})$ and the constraint in (14b) is not jointly convex in $(\boldsymbol{Q}, \boldsymbol{\Gamma})$. The rest of this work proposes two iterative schemes to tackle (14), one that employs the sequential fractional programming framework together with a reformulation of the RHS optimization problem, and another one that performs the optimization of $\boldsymbol{Q}$ based on a search in a standard-compliant codebook. The former will have stronger optimality claims and better performance, but also higher complexity. The proposed approach to tackle (14) leverages on the alternating optimization framework, treating separately the optimization of the reflection matrix $\boldsymbol{\Gamma}$ and of the transmit covariance matrix $\boldsymbol{Q}$. The optimization of the metasurface will be treated in Sec. 3, while two approaches for the optimization of the transmit covariance matrix will be discussed in Sect. 4.

3 RHS optimization for EE maximization

Since the denominator of the EE does not depend on $\boldsymbol{\Gamma}$, the optimization of $\boldsymbol{\Gamma}$, for fixed $\boldsymbol{Q}$, reduces to the maximization of the system capacity, namely

$$\max_{\boldsymbol{\Gamma}} \log_2\left|\boldsymbol{I} + \frac{1}{\sigma^2}\boldsymbol{G\Gamma A\Gamma}^H\boldsymbol{G}^H\right| \tag{15a}$$

$$\text{s.t. } \mathrm{tr}(\boldsymbol{\Gamma A\Gamma}^H) \leq \mathrm{tr}(\boldsymbol{A}), \tag{15b}$$

wherein we have defined $\boldsymbol{A} = \boldsymbol{H Q H}^H$. Problem (15) is a non-convex problem, due to the non-concavity of[1] (15a). In order to tackle it, let us express the matrix $\boldsymbol{A}$ through its eigenvalue decomposition, namely

[1] Indeed, in the special case of a single-antenna system and a metasurface with only one reflecting element γ, (15) would reduce to $\log_2(1 + g^2a^2|\gamma|^2)$, with ga the equivalent SISO channel gain. Clearly, not even in this simplified special case (15) is concave in γ.

$$\boldsymbol{A} = \sum_{\ell=1}^{N} \lambda_\ell \boldsymbol{u}_\ell \boldsymbol{u}_\ell^H, \tag{16}$$

with λ_ℓ and $\boldsymbol{u}_\ell$ the ℓ-th eigenvalue and eigenvector of $\boldsymbol{HQH}^H$. Then, it holds

$$\begin{aligned} \boldsymbol{\Gamma A \Gamma}^H &= \boldsymbol{\Gamma} \left(\sum_{\ell=1}^{N} \lambda_\ell \boldsymbol{u}_\ell \boldsymbol{u}_\ell^H \right) \boldsymbol{\Gamma}^H = \left(\sum_{\ell=1}^{N} \lambda_\ell \boldsymbol{\Gamma} \boldsymbol{u}_\ell \boldsymbol{u}_\ell^H \boldsymbol{\Gamma}^H \right) \\ &= \left(\sum_{\ell=1}^{N} \lambda_\ell \boldsymbol{U}_\ell \boldsymbol{\gamma} \boldsymbol{\gamma}^H \boldsymbol{U}_\ell^H \right), \end{aligned} \tag{17}$$

wherein $\boldsymbol{U}_\ell = \mathrm{diag}(\boldsymbol{u}_\ell)$, $\boldsymbol{\gamma} = [\gamma_{1,1}, \ldots, \gamma_{N,N}]^T$, and we have exploited that $\boldsymbol{\Gamma u}_\ell = \mathrm{diag}(\boldsymbol{u}_\ell)\boldsymbol{\gamma} = \boldsymbol{U}_\ell \boldsymbol{\gamma}$. Then, Problem (15) can be restated as

$$\max_{\boldsymbol{\gamma}} \log_2 \left| \boldsymbol{I} + \frac{1}{\sigma^2} \boldsymbol{G} \left(\sum_{\ell=1}^{N} \lambda_\ell \boldsymbol{U}_\ell \boldsymbol{\gamma} \boldsymbol{\gamma}^H \boldsymbol{U}_\ell^H \right) \boldsymbol{G}^H \right| \tag{18a}$$

$$\text{s.t.} \sum_{\ell=1}^{N} \lambda_\ell \mathrm{tr}\left(\boldsymbol{U}_\ell \boldsymbol{\gamma} \boldsymbol{\gamma}^H \boldsymbol{U}_\ell^H \right) \leq \mathrm{tr}(\boldsymbol{A}). \tag{18b}$$

Problem (18) is still challenging, since the objective is still not concave in $\boldsymbol{\gamma}$. On the other hand, it is concave in $\boldsymbol{\gamma}\boldsymbol{\gamma}^H$, which would suggest to employ the semidefinite relaxation method. However, this has the drawback of possibly requiring a rank reduction step, which might degrade the performance, leaving us without any guarantee as to the efficiency of the optimized matrix $\boldsymbol{\Gamma}$. For this reason, here we resort to a different approach. First, we still introduce the new variable $\boldsymbol{R} = \boldsymbol{\gamma}\boldsymbol{\gamma}^H$, but, unlike what the semidefinite relaxation method does, we do not relax the rank-one constraint on $\boldsymbol{R}$, but instead we equivalently reformulate it in a more tractable way. To elaborate, defining $\boldsymbol{R} = \boldsymbol{\gamma}\boldsymbol{\gamma}^H$, leads to the problem

$$\max_{\boldsymbol{R} \succeq \boldsymbol{0}, \boldsymbol{\gamma}} \log_2 \left| \boldsymbol{I} + \frac{1}{\sigma^2} \boldsymbol{G} \left(\sum_{\ell=1}^{N} \lambda_\ell \boldsymbol{U}_\ell \boldsymbol{R} \boldsymbol{U}_\ell^H \right) \boldsymbol{G}^H \right| \tag{19a}$$

$$\text{s.t.} \sum_{\ell=1}^{N} \lambda_\ell \mathrm{tr}\left(\boldsymbol{U}_\ell \boldsymbol{R} \boldsymbol{U}_\ell^H \right) \leq \mathrm{tr}(\boldsymbol{A}) \tag{19b}$$

$$\mathrm{rank}(\boldsymbol{R}) = 1 \tag{19c}$$

At this point, we resort to the following result.

1 Proposition 1

Consider the following optimization problem.

$$\max_{\boldsymbol{R}\succeq\mathbf{0},\boldsymbol{\gamma}} \ \log_2 \left| \boldsymbol{I} + \frac{1}{\sigma^2}\boldsymbol{G}\left(\sum_{\ell=1}^{N} \lambda_\ell \boldsymbol{U}_\ell \boldsymbol{R} \boldsymbol{U}_\ell^H\right)\boldsymbol{G}^H \right| \tag{20a}$$

$$\text{s.t.} \ \sum_{\ell=1}^{N} \lambda_\ell \mathrm{tr}\left(\boldsymbol{U}_\ell \boldsymbol{R} \boldsymbol{U}_\ell^H\right) \leq \mathrm{tr}(\boldsymbol{A}) \tag{20b}$$

$$\begin{bmatrix} \boldsymbol{R} & \boldsymbol{\gamma} \\ \boldsymbol{\gamma}^H & 1 \end{bmatrix} \succeq \mathbf{0} \tag{20c}$$

$$\mathrm{tr}(\boldsymbol{R}) \leq \|\boldsymbol{\gamma}\|^2 \tag{20d}$$

Then, any $\boldsymbol{R}$ *that is feasible for Problem* (20)*, has rank equal to* 1 *and so is feasible for Problem* (19)*, too.*

Proof To begin with, let us show that Constraint (20c) implies $\mathbf{R} \succeq \boldsymbol{\gamma}\boldsymbol{\gamma}^H$. To see this we observe that, since $\boldsymbol{R} \succeq \mathbf{0}$, by Sylvester's criterion the leading principal minors of $\boldsymbol{R}$ are greater than or equal to 0. Then, again by Sylvester criterion, the positive semidefiniteness property in (20c) is satisfied if and only if

$$\det \begin{pmatrix} \boldsymbol{R} & \boldsymbol{\gamma} \\ \boldsymbol{\gamma}^H & 1 \end{pmatrix} \geq 0. \tag{21}$$

The determinant can be obtained by applying [45, 0.8.5]:

$$\det \begin{pmatrix} \boldsymbol{R} & \boldsymbol{\gamma} \\ \boldsymbol{\gamma}^H & 1 \end{pmatrix} = \det(\boldsymbol{R} - \boldsymbol{\gamma}\boldsymbol{\gamma}^H) \geq 0. \tag{22}$$

Now, let $\boldsymbol{R} \succ \mathbf{0}$ and $\det(\boldsymbol{R} - \boldsymbol{\gamma}\boldsymbol{\gamma}^H) > 0$. Then,

$$\frac{\det(\boldsymbol{R} - \boldsymbol{\gamma}\boldsymbol{\gamma}^H)}{\det(\boldsymbol{R})} = \det(\boldsymbol{I} - \boldsymbol{R}^{-1/2}\boldsymbol{\gamma}\boldsymbol{\gamma}^H\boldsymbol{R}^{-1/2}) > 0. \tag{23}$$

Since $\boldsymbol{R}^{-1/2}\boldsymbol{\gamma}\boldsymbol{\gamma}^H\boldsymbol{R}^{-1/2}$ has unit rank, the eigenvalues of $\boldsymbol{I} - \boldsymbol{R}^{-1/2}\boldsymbol{\gamma}\boldsymbol{\gamma}^H\boldsymbol{R}^{-1/2}$ are 1, with multiplicity $N_R - 1$, and $1 - \boldsymbol{\gamma}^H\boldsymbol{R}^{-1}\boldsymbol{\gamma}$. Then, this matrix is positive definite and, after multiplying on the left and on the right by $\boldsymbol{R}^{1/2}$, we get $\mathbf{R} \succ \boldsymbol{\gamma}\boldsymbol{\gamma}^H$. If $\boldsymbol{R} \succeq \mathbf{0}$ (positive semidefinite), define $\boldsymbol{R}_n \triangleq (1/n)\boldsymbol{I} + \boldsymbol{R}$ and consider the sequence $\lambda_n \triangleq \lambda_{\min}(\boldsymbol{R}_n - \boldsymbol{\gamma}\boldsymbol{\gamma}^H)$. By the Monotone Convergence Theorem, this sequence is positive and monotonically decreasing, so that $\lim_{n\to\infty} \lambda_n \geq 0$. Finally, the continuity of the eigenvalue function completes the proof of our statement. Then, assuming without loss of generality that the eigenvalues of $\boldsymbol{R}$, say $\lambda_{R,1}, \ldots, \lambda_{R,N}$, are ordered in decreasing order of magnitude, (20c) implies that

$$\lambda_{R,1} \geq \|\boldsymbol{\gamma}\|^2, \tag{24}$$

whereas (20d) requires that

$$\sum_{i=1}^{N} \lambda_{R,i} = \lambda_{R,1} + \sum_{2=1}^{N} \lambda_{R,i} \leq \|\boldsymbol{\gamma}\|^2. \tag{25}$$

Thus, since $\lambda_{R,i} \geq 0$ for all $i = 1, \ldots, N$, (20c) and (20d) together imply that $\lambda_{R,1} = \|\boldsymbol{\gamma}\|^2$ and $\lambda_{R,i} = 0$ for all $i = 2, \ldots, N$. Hence, the thesis. □

Despite the above result, Problem (20) is still non-convex, due to the non-convex constraint (20d). However, Problem (20) is more tractable than (19), because the functions in the non-convex constraint (20d) are differentiable, while the rank function in (19) is not. This allows us to resort to the sequential programming framework to develop an iterative algorithm that monotonically improves the objective value of (20), eventually converging to a first-order optimal point of (20). The fundamentals of sequential programming can be found in [46], and are reviewed in Appendix A.

In order to apply the sequential programming framework to (20), we exploit the fact that $\|\boldsymbol{\gamma}\|^2$ is a convex function, and thus it is lower-bounded by its first-order Taylor expansion around any given point $\bar{\boldsymbol{\gamma}}$, namely

$$\|\boldsymbol{\gamma}\|^2 \geq \|\bar{\boldsymbol{\gamma}}\|^2 + 2\Re\{\bar{\boldsymbol{\gamma}}^H(\boldsymbol{\gamma} - \bar{\boldsymbol{\gamma}})\} = 2\Re\{\bar{\boldsymbol{\gamma}}^H\boldsymbol{\gamma}\} - \|\bar{\boldsymbol{\gamma}}\|^2 \tag{26}$$

Then, a surrogate problem for (20), which fulfills the assumptions of the sequential optimization framework is obtained as[2]

$$\max_{\boldsymbol{R}\succeq\boldsymbol{0},\boldsymbol{\gamma}} \ \log_2 \left| \boldsymbol{I} + \frac{1}{\sigma^2}\boldsymbol{G}\left(\sum_{\ell=1}^{N} \lambda_\ell \boldsymbol{U}_\ell \boldsymbol{R} \boldsymbol{U}_\ell^H\right)\boldsymbol{G}^H \right| \tag{27a}$$

$$\text{s.t.} \ \sum_{\ell=1}^{N} \lambda_\ell \mathrm{tr}\left(\boldsymbol{U}_\ell \boldsymbol{R} \boldsymbol{U}_\ell^H\right) \leq \mathrm{tr}(\boldsymbol{H}\boldsymbol{Q}\boldsymbol{H}^H) \tag{27b}$$

$$\begin{bmatrix} \boldsymbol{R} & \boldsymbol{\gamma} \\ \boldsymbol{\gamma}^H & 1 \end{bmatrix} \succeq \boldsymbol{0} \tag{27c}$$

$$\mathrm{tr}(\boldsymbol{R}) - 2\Re\{\bar{\boldsymbol{\gamma}}^H\boldsymbol{\gamma}\} + \|\bar{\boldsymbol{\gamma}}\|^2 \leq 0\,, \tag{27d}$$

and a sequential optimization algorithm to tackle (20) is obtained as in Algorithm 1.

Algorithm 1 RHS optimization

1: Choose $\varepsilon > 0$;
2: Set $\bar{\boldsymbol{\gamma}}$ to a feasible value;
3: **repeat**
4: Solve (27) and denote its solution by $(\boldsymbol{R}^\star, \boldsymbol{\gamma}^\star)$;
5: $\mathrm{Err} = |\boldsymbol{\gamma}^\star - \bar{\boldsymbol{\gamma}}|$;
6: $\bar{\boldsymbol{\gamma}} = \boldsymbol{\gamma}^\star$;
7: **until** $\mathrm{Err} \leq \varepsilon$

[2] Notice that inequality (27d) implies (20d), according to the requirements of the sequential method.

4 Transmit covariance optimization

4.1 Optimization by fractional programming

The optimization with respect to $\boldsymbol{Q}$, for fixed $\boldsymbol{\Gamma}$, is cast as

$$\max_{\boldsymbol{Q}} \frac{\log_2 \left| \boldsymbol{I} + \frac{1}{\sigma^2} \boldsymbol{G}\boldsymbol{\Gamma}\boldsymbol{H}\boldsymbol{Q}\boldsymbol{H}^H\boldsymbol{\Gamma}^H\boldsymbol{G}^H \right|}{\mu \mathrm{tr}(\boldsymbol{Q}) + P_c} \tag{28a}$$

$$\text{s.t. } \mathrm{tr}(\boldsymbol{\Gamma}\boldsymbol{H}\boldsymbol{Q}\boldsymbol{H}^H\boldsymbol{\Gamma}^H) \leq \mathrm{tr}(\boldsymbol{H}\boldsymbol{Q}\boldsymbol{H}^H) \tag{28b}$$

$$\mathrm{tr}(\boldsymbol{Q}) \leq P_{max}. \tag{28c}$$

Problem (28) is a fractional maximization program, in which the fractional objective has a concave numerator and an affine denominator, while the constraint functions are also affine. Thus, (28) can be solved by direct use of fractional programming methods [47], e.g. Dinkelbach's algorithm. However, it should be noted that, unlike typical EE maximization problems in MIMO links, Problem (28) does not allow the diagonalization of the covariance matrix $\boldsymbol{Q}$, due to the presence of (28b), in which there is no multiplication by the matrix $\boldsymbol{G}$, as it happens in (28a). This is a direct consequence of the consideration of RHSs with global reflection constraints, which leads to (28b). Dinkelbach's algorithm to solve (28) can be stated as in Algorithm 2.

Algorithm 2 Dinkelbach's algorithm for Problem (28)

1: Set $\lambda_{new} = 0$, $\varepsilon > 0$;
2: **repeat**
3: Let $\boldsymbol{Q}^\star$ be the solution of the following Problem

$$\max_{\boldsymbol{Q}} \log_2 \left| \boldsymbol{I} + \frac{1}{\sigma^2} \boldsymbol{G}\boldsymbol{\Gamma}\boldsymbol{H}\boldsymbol{Q}\boldsymbol{H}^H\boldsymbol{\Gamma}^H\boldsymbol{G}^H \right| - \lambda(\mu \mathrm{tr}(\boldsymbol{Q}) + P_c) \tag{29a}$$

$$\text{s.t. } \mathrm{tr}(\boldsymbol{\Gamma}\boldsymbol{H}\boldsymbol{Q}\boldsymbol{H}^H\boldsymbol{\Gamma}^H) \leq \mathrm{tr}(\boldsymbol{H}\boldsymbol{Q}\boldsymbol{H}^H) \tag{29b}$$

$$\mathrm{tr}(\boldsymbol{Q}) \leq P_{max}. \tag{29c}$$

4: $\lambda_{old} = \lambda_{new}$;
5:

$$\lambda_{new} = \frac{\log_2 \left| \boldsymbol{I} + \frac{1}{\sigma^2} \boldsymbol{G}\boldsymbol{\Gamma}\boldsymbol{H}\boldsymbol{Q}^\star\boldsymbol{H}^H\boldsymbol{\Gamma}^H\boldsymbol{G}^H \right|}{\mu \mathrm{tr}(\boldsymbol{Q}^\star) + P_c} \tag{30}$$

6: **until** $|\lambda_{new} - \lambda_{old}| \leq \varepsilon$

Finally, an alternating optimization algorithm for Problem (14) can be formulated as in Algorithm 3, for which the following result holds.

1 Proposition 2

Algorithm 3 *monotonically increases the value of the objective in* (14*a*) *and converges.*

1 ***Proof***

Algorithm 3 iteratively applies the sequential optimization method to optimize $\mathbf{\Gamma}$ *and Dinkelbach's algorithm to optimize* $\mathbf{Q}$*. The former is known to monotonically increase the value of the objective, while the latter is provably optimal. Thus, after solving each subproblem of Algorithm 3, the EE function is not decreased. Then, let us observe that EE is an upper-bounded function. Indeed, it is continuous in the eigenvalues of* $\mathbf{Q}$*, and it is equal to zero both when* $\mathrm{tr}(\mathbf{Q}) = 0$*, and* $\mathrm{tr}(\mathbf{Q}) \to \infty$*. Therefore, there must exist finite eigenvalues of* $\mathbf{Q}$ *such that the EE takes the maximum value. This implies that the EE value cannot increase indefinitely and thus Algorithm 3 must converge in the value of the objective.* □

Algorithm 3 EE maximization

Choose $\varepsilon > 0$;
Set $(\boldsymbol{Q}_0, \mathbf{\Gamma}_0)$ to feasible values;
repeat
  Let $\mathbf{\Gamma}$ be the output of Algorithm 1, given $\boldsymbol{Q}_0$;
  Let $\boldsymbol{Q}$ be the output of Algorithm 2, given $\mathbf{\Gamma}$;
  $\mathrm{Err} = |\mathrm{EE}(\mathbf{\Gamma}, \boldsymbol{Q}) - \mathrm{EE}(\mathbf{\Gamma}_0, \boldsymbol{Q}_0)|$;
  $\boldsymbol{Q}_0 = \boldsymbol{Q}$; $\mathbf{\Gamma}_0 = \mathbf{\Gamma}$;
until $\mathrm{Err} \leq \varepsilon$

1 ***Remark 2***

Algorithm 3 can be specialized to perform capacity maximization instead of EE maximization by simply setting $\mu = 0$ *in (14a). Indeed, this turns the denominator of (14a) into a constant, thus reducing the problem to the maximization of the capacity in the numerator of (14a).*

4.2 Optimization by codebook search

As for covariance matrix optimization, aiming at a lower-complexity optimization approach, we also propose an approach based on the use of standard-compliant codebooks, considering Type-I and Type-II codebooks, which define the beamforming vectors based on a discrete Fourier transform sampling. Specifically, let us consider a cross-polarization single-panel antenna array with (N_1, N_2) denoting the number of antenna elements along horizontal and vertical axes in a single polarization. Thus, the aggregate count of transmit antenna elements is $2N_1N_2$, accounting for polarization diversity. Introducing the oversampling factors (O_1, O_2) enables the construction of a beam grid based on two-dimensional (2D) DFT principles [48]. Namely, for $i = 1, 2$, the oversampled DFT beams in one orientation can be formulated as follows:

$$\begin{aligned}&\boldsymbol{\mu}^i(\theta_i) = \left[\begin{array}{cccc} 1 & e^{j\frac{2\pi\theta_i}{N_iO_i}} & \cdots & e^{j\frac{2\pi\theta_i(N_i-1)}{N_iO_i}} \end{array}\right]^T, \\ &\theta_i \in \{0, 1, \ldots, N_iO_i - 1\},\end{aligned} \tag{31}$$

where θ_i are beam indexes along the horizontal ($i = 1$) and vertical ($i = 2$) directions. Based on the antenna configuration and oversampling ratios specified in [49], a series of 2D DFT spatial domain beams is generated:

$$\mathcal{D} = \left\{\boldsymbol{b}_{\theta_1,\theta_2} \mid \boldsymbol{b}_{\theta_1,\theta_2} = \boldsymbol{\mu}^1(\theta_1) \otimes \boldsymbol{\mu}^2(\theta_2)\right\}, \tag{32}$$

with $\otimes$ denoting the Kronecker product. Here, $\boldsymbol{b}_{\theta_1,\theta_2} \in \mathbb{C}^{N_1N_2\times 1}$ represents an oversampled 2D DFT beam, and $|\mathcal{D}| = N_1O_1 \times N_2O_2$.

Through beam selection and phase tuning, the Type I codebook $\mathcal{C}_I$ is derived, whereas the Type II codebook $\mathcal{C}_{II}$ emerges from selecting a subset of beams and adjusting their linear combination coefficients for beam fusion [50], employing identical subsets across polarizations. For single-stream transmission, the Type I codebook vectors are written as:

$$\boldsymbol{w}_{\mathrm{I}}(\theta_1, \theta_2) = \frac{1}{\sqrt{2N_1N_2}}\left[\begin{array}{c} \boldsymbol{b}_{\theta_1,\theta_2} \\ \varphi\boldsymbol{b}_{\theta_1,\theta_2} \end{array}\right], \tag{33}$$

wherein the scalar $\varphi \in \{1, j, -1, -j\}$ accounts for the phase difference across two polarization directions. The definition of w_{I} relies on the parameters φ, θ_1, and θ_2, leading to a codebook with a total of $4 \times N_1O_1 \times N_2O_2$ possible vectors w_{I}, with the factor 4 accounting for the fact that φ takes values in the set $\{1, j, -1, -j\}$.

For single-stream transmission based on the combination of K beams, the Type II codebook is represented by:

$$\boldsymbol{w}_{\mathrm{II}}(\boldsymbol{\theta}_1, \boldsymbol{\theta}_2) = \left[\begin{array}{c} \sum_{i=0}^{K-1} \boldsymbol{b}_{\theta_1^{(i)},\theta_2^{(i)}} p_{1,i}^{\mathrm{WB}} p_{1,i}^{\mathrm{SB}} c_{1,i} \\ \sum_{i=0}^{K-1} \boldsymbol{b}_{\theta_1^{(i)},\theta_2^{(i)}} p_{2,i}^{\mathrm{WB}} p_{2,i}^{\mathrm{SB}} c_{2,i} \end{array}\right], \tag{34}$$

where $\boldsymbol{\theta}_1 \triangleq (\theta_1^{(i)})_{i=1}^K$ and $\boldsymbol{\theta}_2 \triangleq (\theta_2^{(i)})_{i=1}^K$. Each element encapsulates a linear blend of K beams from $\mathcal{D}$ for a given polarization. The coefficients $p_{\ell,i}^{\mathrm{WB}}$, $p_{\ell,i}^{\mathrm{SB}}$, and $c_{\ell,i}$ correspond to the wideband amplitude combination, subband amplitude combination, and phase combination for polarization ℓ, where $\ell = 1, 2$, and beam i, respectively. The procedure for merging K beams to approximate the wideband channel information as closely as possible involves the use of a wideband beam combining coefficient matrix. This matrix's amplitudes are normalized based on the strongest beam, which is quantized with a 3-bit scheme to yield $p_{\ell,i}^{\mathrm{WB}}$ [49].

Finally, we can build the transmit covariance matrix by searching in the codebook (either Type-I or Type-II) the optimal beamforming vector. To elaborate, for any beaforming vector in the codebook, we can form the covariance matrix $\boldsymbol{Q}_\ell = a\widetilde{\boldsymbol{Q}}_\ell$, with $\widetilde{\boldsymbol{Q}}_\ell = \boldsymbol{w}_\ell\boldsymbol{w}_\ell^H$, with $\ell = 1$ for Type-I codebooks and $\ell = 2$ for Type-II codebooks. We also note that the codebook is constructed in order to have $\mathrm{tr}(\boldsymbol{Q}_\ell) = a$, which means that the EE can be rewritten as

$$\mathrm{EE} = \frac{\log_2 \left| \boldsymbol{I} + \frac{a}{\sigma^2} \boldsymbol{G}\boldsymbol{\Gamma}\boldsymbol{H}\widetilde{\boldsymbol{Q}}_\ell \boldsymbol{H}^H \boldsymbol{\Gamma}^H \boldsymbol{G}^H \right|}{\mu a + P_c}, \tag{35}$$

Thus, $\widetilde{\boldsymbol{Q}}_\ell$ and the scalar a can be found by solving

$$\max_{a,\widetilde{\boldsymbol{Q}}_\ell} \frac{\log_2 \left| \boldsymbol{I} + \frac{a}{\sigma^2} \boldsymbol{G}\boldsymbol{\Gamma}\boldsymbol{H}\widetilde{\boldsymbol{Q}}_\ell \boldsymbol{H}^H \boldsymbol{\Gamma}^H \boldsymbol{G}^H \right|}{\mu a + P_c} \tag{36a}$$

$$\text{s.t. } \mathrm{tr}(\boldsymbol{\Gamma}\boldsymbol{H}\widetilde{\boldsymbol{Q}}_\ell \boldsymbol{H}^H \boldsymbol{\Gamma}^H) \leq \mathrm{tr}(\boldsymbol{H}\widetilde{\boldsymbol{Q}}_\ell \boldsymbol{H}^H) \tag{36b}$$

$$a \leq P_{max}. \tag{36c}$$

Problem (36) can be solved by searching for $\widetilde{\boldsymbol{Q}}_\ell$ in the codebook (either Type-I or Type-II), which has cardinality proportional to $N_T O_1 O_2$. For each candidate matrix $\widetilde{\boldsymbol{Q}}_\ell$ the scalar a can be determined by solving a simple scalar problem. Then, an alternating optimization method based on codebook search can be stated as in Algorithm 4.

Algorithm 4 EE maximization by codebook search

Choose $\varepsilon > 0$;
Set $(\boldsymbol{Q}_0, \boldsymbol{\Gamma}_0)$ to feasible values;
repeat
  Let $\boldsymbol{\Gamma}$ be the output of Algorithm 1, given $\boldsymbol{Q}_0$;
  Let $\boldsymbol{Q}$ be the solution of (36), given $\boldsymbol{\Gamma}$;
  $\mathrm{Err} = |\mathrm{EE}(\boldsymbol{\Gamma}, \boldsymbol{Q}) - \mathrm{EE}(\boldsymbol{\Gamma}_0, \boldsymbol{Q}_0)|$;
  $\boldsymbol{Q}_0 = \boldsymbol{Q}$; $\boldsymbol{\Gamma}_0 = \boldsymbol{\Gamma}$;
until $\mathrm{Err} \leq \varepsilon$

1 ***Remark 3***

As in the case of Algorithm 3, also Algorithm 4 can be specialized to perform capacity maximization instead of EE maximization by simply setting $\mu = 0$ *in (36a).*

1 ***Remark 4***

Algorithm 4 can be seen to have a lower complexity than Algorithm 3. To show this, let us denote by I_{alt} *the number of iterations of Algorithm 3 until convergence. Then Algorithm 3 requires running the sequential optimization method and Dinkelbach's algorithm* I_{alt} *times. In turn, Dinkelbach's algorithm and the sequential algorithm require the solution of* I_{dink} *and* I_{seq} *convex problems, respectively, with* I_{dink} *and* I_{seq} *being the number of iterations until Dinkelbach's algorithm and the sequential algorithm converge. Then, recalling that the complexity of a convex problem can be bounded by the fourth power of the number of variables [51], the overall complexity of Algorithm 3 can be evaluated as*

$$\mathcal{C} = \mathcal{O}\left(I_{alt}\left(I_{seq}N^4 + I_{dink}\left(\frac{N_T(N_T+1)}{2}\right)^4\right)\right), \tag{37}$$

where we have accounted for the fact that the matrix $\boldsymbol{Q}$ is Hermitian and thus has $N_T(N_T+1)/2$ free variables. On the other hand, since the codebook has cardinality proportional to $N_T O_1 O_2$, the complexity of Algorithm 4 can be evaluated as

$$\mathcal{C}_{CB} = \mathcal{O}\Big(I_{alt,CB}\Big(I_{seq,CB}N^4 + N_T O_1 O_2\Big)\Big), \tag{38}$$

wherein $I_{alt,CB}$ and $I_{seq,CB}$ are the number of iterations until convergence of the Algorithm 4 and of the sequential algorithm that is run inside Algorithm 4. Moreover, we also observe that the complexity of the codebook search can be tuned by choosing O_1 and O_2 in order to have a finer or coarser resolution of the codebook.

5 Extension to active RHS

This section discusses how to extend the optimization algorithms discussed in previous sections, to the case in which the RHS at the transmitter is active, i.e. it is equipped with analog amplifiers that enhance the incoming signal [6]. It should be stressed that the amplification takes place in the analog domain, and thus no digital-to-analog conversion is required at the RHS. This motivates the consideration of an active RHS to provide an additional, but cheaper, possibility of amplifying the radio-frequency signal. Analog amplifiers integrated into a metasurface generally exhibit lower quality than traditional amplifiers used in digital transmitters, making them less expensive. In fact, the metasurface compensates for this limitation by offering significant array gain due to its large number of electromagnetic elements. This enables the use of a lower-quality, and thus less expensive, amplifier at the transmitter, with the amplification of the metasurface offsetting the reduced performance. Additionally, we assume the use of an active metasurface with global reflection capabilities, as described in [8, 43].

The fact that the RHS is active affects the reflection constraint at the RHS, since now it is no longer necessary to enforce that $P_{in} \geq P_{out}$. On the other hand, it must hold that $P_{out} \leq P_{in} + P_r$, with P_r the radio-frequency power provided by the RHS amplifier. Moreover, if the RHS is constrained to operate in the active regime, it must also be true that $P_{out} \geq P_{in}$. In addition, the total power consumed by the system should also account for the radio frequency power consumed by the RHS, which is equal to $P_{out} - P_{in}$. Finally, it should also be considered that an active RHS will add thermal noise to the incoming signal due to the analog amplifier. So, denoting by σ^2_{RHS} the power of the thermal noise introduced by the active RHS, the radio-frequency power at the output of the RHS is given by

$$P_{out} = \mathrm{tr}(\boldsymbol{\Gamma}(\boldsymbol{H}\boldsymbol{Q}\boldsymbol{H}^H + \sigma^2_{RHS}\boldsymbol{I})\boldsymbol{\Gamma}^H), \tag{39}$$

and the total power consumed in the system is written as

$$P_t = \mu\,\mathrm{tr}(\boldsymbol{Q}) + P_c + \mathrm{tr}(\boldsymbol{\Gamma}(\boldsymbol{H}\boldsymbol{Q}\boldsymbol{H}^H + \sigma^2_{RHS}\boldsymbol{I})\boldsymbol{\Gamma}^H) - \mathrm{tr}(\boldsymbol{H}\boldsymbol{Q}\boldsymbol{H}^H). \tag{40}$$

Thus, the EE maximization problem with active RHS is stated as

$$\max_{\boldsymbol{\Gamma},\boldsymbol{Q}} \frac{\log_2\left|\boldsymbol{I}+\frac{1}{\sigma^2}\boldsymbol{G}\boldsymbol{\Gamma}(\boldsymbol{H}\boldsymbol{Q}\boldsymbol{H}^H+\sigma_{RHS}^2\boldsymbol{I})\boldsymbol{\Gamma}^H\boldsymbol{G}^H\right|}{\mu\mathrm{tr}(\boldsymbol{Q})+P_c+\mathrm{tr}(\boldsymbol{\Gamma}(\boldsymbol{H}\boldsymbol{Q}\boldsymbol{H}^H+\sigma_{RHS}^2\boldsymbol{I})\boldsymbol{\Gamma}^H)-\mathrm{tr}(\boldsymbol{H}\boldsymbol{Q}\boldsymbol{H}^H)} \tag{41a}$$

$$\text{s.t. } \mathrm{tr}(\boldsymbol{H}\boldsymbol{Q}\boldsymbol{H}^H)\le\mathrm{tr}(\boldsymbol{\Gamma}(\boldsymbol{H}\boldsymbol{Q}\boldsymbol{H}^H\boldsymbol{\Gamma}^H+\sigma_{RHS}^2\boldsymbol{I})\boldsymbol{\Gamma}^H)\le\mathrm{tr}(\boldsymbol{H}\boldsymbol{Q}\boldsymbol{H}^H)+P_r \tag{41b}$$

$$\mathrm{tr}(\boldsymbol{Q})\le P_{max}\ . \tag{41c}$$

With respect to $\boldsymbol{Q}$, the problem is still a pseudo-concave maximization, which can be solved optimally by Dinkelbach's method, and heuristically by applying the codebook approach, as discussed in Sect. 4. As for the optimization of $\boldsymbol{\Gamma}$, it is now stated as the fractional problem

$$\max_{\boldsymbol{\Gamma},\boldsymbol{Q}} \frac{\log_2\left|\boldsymbol{I}+\frac{1}{\sigma^2}\boldsymbol{G}\boldsymbol{\Gamma}\boldsymbol{A}\boldsymbol{\Gamma}^H\boldsymbol{G}^H\right|}{\mathrm{tr}(\boldsymbol{\Gamma}\boldsymbol{A}\boldsymbol{\Gamma}^H)+P_{c,eq}} \tag{42a}$$

$$\text{s.t. } \mathrm{tr}(\boldsymbol{H}\boldsymbol{Q}\boldsymbol{H}^H)\le\mathrm{tr}(\boldsymbol{\Gamma}\boldsymbol{A}\boldsymbol{\Gamma}^H)\le\mathrm{tr}(\boldsymbol{H}\boldsymbol{Q}\boldsymbol{H}^H)+P_r\ , \tag{42b}$$

wherein $P_{c,eq}=P_c+\mu\mathrm{tr}(\boldsymbol{Q})-\mathrm{tr}(\boldsymbol{H}\boldsymbol{Q}\boldsymbol{H}^H)$ and $\boldsymbol{A}=\boldsymbol{H}\boldsymbol{Q}\boldsymbol{H}^H+\sigma_{RHS}^2\boldsymbol{I}$. Problem (42) can be tackled by the sequential optimization method, by a similar approach as discussed in Sect. 3. Indeed, following similar steps as in Sect. 3, Problem (42) can be equivalently reformulated as

$$\max_{\boldsymbol{R}\succeq\boldsymbol{0},\boldsymbol{\gamma}} \frac{\log_2\left|\boldsymbol{I}+\frac{1}{\sigma^2}\boldsymbol{G}\left(\sum_{\ell=1}^N\lambda_\ell\boldsymbol{U}_\ell\boldsymbol{R}\boldsymbol{U}_\ell^H\right)\boldsymbol{G}^H\right|}{\sum_{\ell=1}^N\lambda_\ell\mathrm{tr}\left(\boldsymbol{U}_\ell\boldsymbol{R}\boldsymbol{U}_\ell^H\right)+P_{c,eq}} \tag{43a}$$

$$\text{s.t. } \mathrm{tr}(\boldsymbol{H}\boldsymbol{Q}\boldsymbol{H}^H)\le\sum_{\ell=1}^N\lambda_\ell\mathrm{tr}\left(\boldsymbol{U}_\ell\boldsymbol{R}\boldsymbol{U}_\ell^H\right)\le\mathrm{tr}(\boldsymbol{H}\boldsymbol{Q}\boldsymbol{H}^H)+P_r \tag{43b}$$

$$\begin{bmatrix}\boldsymbol{R} & \boldsymbol{\gamma}\\ \boldsymbol{\gamma}^H & 1\end{bmatrix}\succeq\boldsymbol{0} \tag{43c}$$

$$\mathrm{tr}(\boldsymbol{R})\le\|\boldsymbol{\gamma}\|^2\ , \tag{43d}$$

wherein $\boldsymbol{U}_\ell=\mathrm{diag}(\boldsymbol{u}_\ell)$, with $\boldsymbol{u}_\ell$ and λ_ℓ the ℓ-th eigenvector and eigenvalue of $\boldsymbol{A}$. Problem (43) can be tackled by the sequential optimization framework, considering, in each iteration, the surrogate problem

$$\max_{\boldsymbol{R}\succeq\boldsymbol{0},\boldsymbol{\gamma}} \frac{\log_2\left|\boldsymbol{I}+\frac{1}{\sigma^2}\boldsymbol{G}\left(\sum_{\ell=1}^N\lambda_\ell\boldsymbol{U}_\ell\boldsymbol{R}\boldsymbol{U}_\ell^H\right)\boldsymbol{G}^H\right|}{\sum_{\ell=1}^N\lambda_\ell\mathrm{tr}\left(\boldsymbol{U}_\ell\boldsymbol{R}\boldsymbol{U}_\ell^H\right)+P_{c,eq}} \tag{44a}$$

$$\text{s.t. } \mathrm{tr}(\boldsymbol{H}\boldsymbol{Q}\boldsymbol{H}^H)\le\sum_{\ell=1}^N\lambda_\ell\mathrm{tr}\left(\boldsymbol{U}_\ell\boldsymbol{R}\boldsymbol{U}_\ell^H\right)\le\mathrm{tr}(\boldsymbol{H}\boldsymbol{Q}\boldsymbol{H}^H)+P_r \tag{44b}$$

$$\begin{bmatrix} \boldsymbol{R} & \boldsymbol{\gamma} \\ \boldsymbol{\gamma}^H & 1 \end{bmatrix} \succeq \mathbf{0} \tag{44c}$$

$$\mathrm{tr}(\boldsymbol{R}) - 2\Re\{\bar{\boldsymbol{\gamma}}^H \boldsymbol{\gamma}\} + \|\bar{\boldsymbol{\gamma}}\|^2 \leq 0\,. \tag{44d}$$

Problem (44) is a pseudo-concave maximization in which the fractional objective has a concave numerator and linear denominator, while all constraints are in convex form. Thus, Problem (44) can be solved globally and efficiently by Dinkelbach's algorithm.

6 Numerical results

For our numerical analysis, we have considered a BS with $N_T = 8$ antennas that communicates with a mobile receiver equipped with $N_R = 2$ antennas, which is located at a distance of 100 m from the BS. We assume that the $N_T = 8$ antennas are deployed in a rectangular 4×2 grid, and uniformly spaced at a distance of $\lambda/2$ from each other. Thus, considering a carrier frequency is 3.5 GHz, the Fraunhofer distance is $r \approx 68$ cm. The BS is placed at a height of 10 m from the ground, while the user equipment is placed at a height of 1.5 m. The communication bandwidth is 20 MHz, the thermal noise power spectral density is -174 dBm/Hz, the noise figure at the receiver is 5 dB. The RHS has $N = 64$ reflecting elements, each consuming a power of $P_{c,n} = 0$ dBm. The rest of the system static power consumption is $N_T P_{c,t} + N_R P_{c,r} + P_{c,0} = 57$ dBm. Figure 1 shows the EE versus the maximum transmit power P_{max} for the following scenarios:

- Optimization of $\boldsymbol{Q}$ and $\boldsymbol{\Gamma}$ for EE maximization by the proposed Algorithm 3
- Optimization of $\boldsymbol{Q}$ and $\boldsymbol{\Gamma}$ for capacity maximization by the proposed Algorithm 3, specialized to perform capacity maximization, as discussed in Remark 2.
- Optimization of $\boldsymbol{Q}$ and $\boldsymbol{\Gamma}$ for EE maximization by the proposed Algorithm 4
- Optimization of $\boldsymbol{Q}$ and $\boldsymbol{\Gamma}$ for capacity maximization by the proposed Algorithm 4, specialized to perform capacity maximization, as discussed in Remark 3.
- Optimization of $\boldsymbol{Q}$ for EE maximization by codebook search and random $\boldsymbol{\Gamma}$. This scheme serves as a benchmark to evaluate the performance loss if RHS optimization is not performed.
- Optimization of $\boldsymbol{Q}$ for capacity maximization by codebook search and random $\boldsymbol{\Gamma}$. This scheme serves as a benchmark to evaluate the performance loss if RHS optimization is not performed.
- Full power allocation, by splitting the power P_{max} uniformly and independently among the transmit antennas, and random $\boldsymbol{\Gamma}$. This scheme is used as a benchmark to evaluate the performance loss if neither $\boldsymbol{Q}$ nor $\boldsymbol{\Gamma}$ are optimized.

As for Algorithm 4, we set $O_1 = 4$ and $O_2 = 1$. The results show that the proposed algorithms are effective in increasing the EE compared to the benchmark scenarios in which no optimization is performed. As expected, the codebook search suffers a penalty compared to the optimal allocation of $\boldsymbol{Q}$ by Dinkelbach's method. However, the gap is limited, especially in the region of interest where the EE reaches its maximum value. This

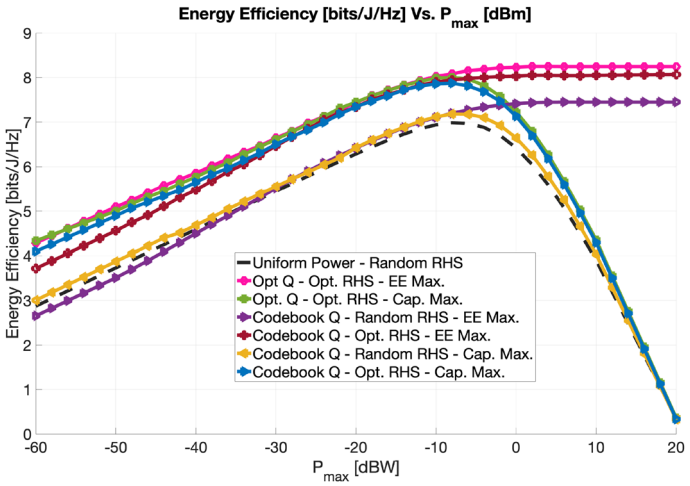

Fig. 1 EE versus maximum available transmit power P_{max} for different resource allocation policies

supports the use of the codebook search in place of the more complex optimization by Dinkelbach's method. Moreover, it is seen that the EE obtained for resource allocations that maximize the capacity lead to a decrease of the EE for larger values of P_{max}. This happens because the EE is not monotonically increasing with P_{max}, while maximizing the capacity always leads to using all of the available power P_{max}. For the same reason, the resource allocations that optimize the EE saturate for larger P_{max} because when P_{max} is large enough to reach the peak of the EE, further increasing the transmit power would only lead to a decrease of the EE.

Figure 2 shows a similar setup as Fig. 1, but the metric that is shown is the system capacity, instead of the EE. Similar considerations as in Fig. 1 holds. In particular, it is found that the proposed optimization schemes lead to significant gains over the benchmark schemes that do not optimize either the RHS matrix or the transmit covariance matrix. Moreover, it is seen that the resource allocations that optimize the EE saturate for larger P_{max}, while the resource allocations that aim at capacity maximization are monotonically increasing, since they employ all of the available transmit power. In Fig. 2 we also see that the codebook-based resource allocation has a more visible difference with respect to the optimization of $\boldsymbol{Q}$ by Algorithm 3 than in the case of EE maximization. Nevertheless, the gap is still limited and justifies the use of the codebook search for complexity reasons.

Next, we address the sensitivity of the proposed Algorithms 3 and 4 to imperfect channel knowledge at the transmitter. To this end, let us consider that the true far-field channel $\boldsymbol{G}$ is known up to an error at the transmitter,[3] which then uses $\widehat{\boldsymbol{G}} \neq \boldsymbol{G}$ for resource allocation purposes. Let us define the normalized error variance (NEV) for $\boldsymbol{G}$ as:

[3] We assume that $\boldsymbol{H}$ is perfectly known, since it is a deterministic channel that is not subject to fading.

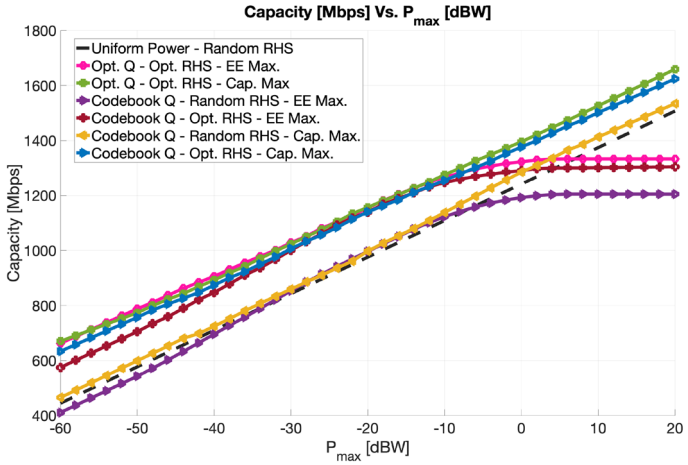

Fig. 2 Capacity versus maximum available transmit power P_{max} for different resource allocation policies

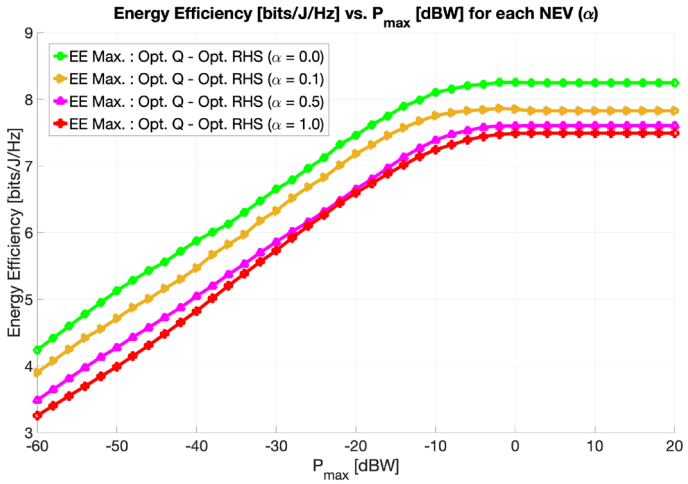

Fig. 3 EE versus P_{max} by Algorithm 3 with imperfect CSI at the transmitter, for different values of α

$$\alpha = \frac{\sum_{n=1}^{N}\sum_{m=1}^{N_R}|G(n,m)-\widehat{G}(n,m)|^2}{\|\widehat{\boldsymbol{G}}\|_F^2/(NN_R)} = \frac{NN_R\|\boldsymbol{G}-\widehat{\boldsymbol{G}}\|_F^2}{\|\widehat{\boldsymbol{G}}\|_F^2} \tag{45}$$

Figures 3 and 4 show the EE achieved by Algorithms 3 and 4 versus P_{max}, respectively, for different values of α. For comparison purposes, the case for $\alpha = 0$, i.e. when $\boldsymbol{G}$ is perfectly known, is also shown. It is seen that the performance degrades as the value of α increases, since estimate $\widehat{\boldsymbol{G}}$ becomes less reliable. However, the performance remains satisfactory even when $\alpha = 1$, thus showing that the proposed algorithms are robust against imperfect channel knowledge.

Figure 5 addresses the impact of the oversampling factors O_1 and O_2 on the EE performance of Algorithm 4. In particular, Fig. 5 shows the EE achieved by Algorithm 4 versus P_{max}, for different choices of the O_1 and O_2. The results indicate that increasing the oversampling factors brings very little performance improvement. Specifically, a visible, although limited, performance improvement is obtained when $O_1 = O_2 = 2$, compared to setting $O_1 = O_2 = 1$. However, further increasing the values of

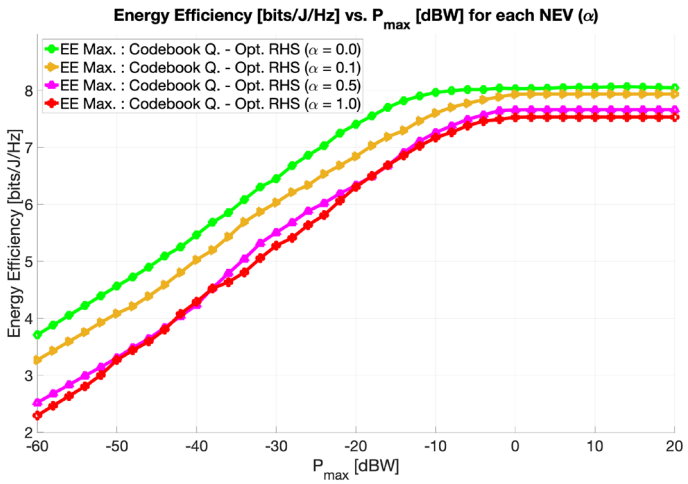

Fig. 4 EE versus P_{max} by Algorithm 4 with imperfect CSI at the transmitter, for different values of α

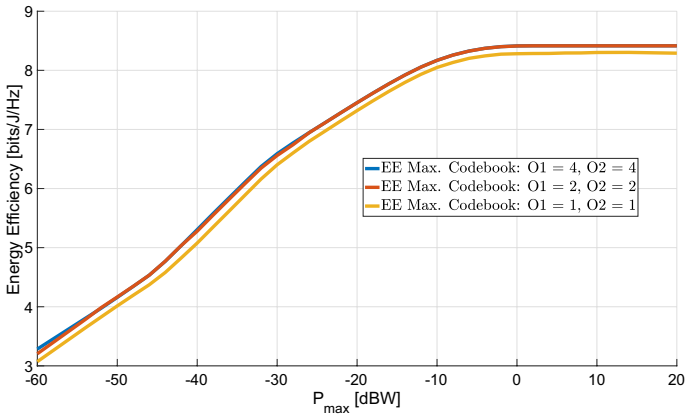

Fig. 5 EE versus P_{max} by Algorithm 4 for different oversampling factors

$O_1 = O_2 = 2$ leads to a negligible performance gain, which suggests to not increase O_1 and O_2 further, as it would only increase the computational complexity, without bringing any significant gain.

The last two figures address the impact of the number of RHS elements N. For these figures, we set $N_T = 4$ and $N_R = 1$. Figure 6 shows the capacity versus the number N of RHS reflecting elements, achieved, for $P_{max} = 40$ dBm, by the following schemes:

- Optimization of $\boldsymbol{Q}$ and $\boldsymbol{\Gamma}$ for capacity maximization by the proposed Algorithm 3 (labeled Opt. $\boldsymbol{Q}$ - Opt. RHS).
- Optimization of $\boldsymbol{Q}$ and $\boldsymbol{\Gamma}$ for capacity maximization by the proposed Algorithm 4.
- Optimization of $\boldsymbol{Q}$ for capacity maximization by Dinkelbach's algorithm and random $\boldsymbol{\Gamma}$ (labeled Opt. $\boldsymbol{Q}$ - Random RHS).
- Optimization of $\boldsymbol{Q}$ for capacity maximization by codebook search and random $\boldsymbol{\Gamma}$.
- Optimization of $\boldsymbol{\Gamma}$ for capacity maximization and uniform and independent power allocation among the transmit antennas.

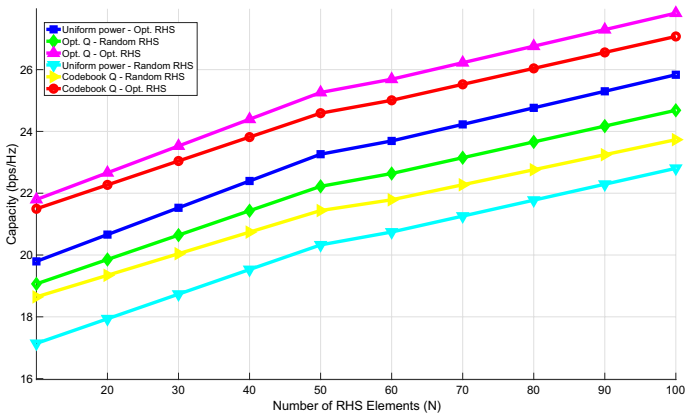

Fig. 6 Capacity versus number of reflecting elements of the RHS for different resource allocation policies

- Random $\boldsymbol{\Gamma}$ and uniform and independent power allocation among the transmit antennas.

As expected the capacity increases with the number of RHS reflecting elements, and the best results are provided by Algorithm 3. Nevertheless, Algorithm 4 entails a limited performance degradation compared to Algorithm 3. Moreover, it is shown that both algorithms can increase the capacity compared to simpler schemes that do not perform any optimization, or that optimize only either the RHS or $\boldsymbol{Q}$.

Finally, Fig. 7 shows the EE versus the number N of RHS reflecting elements, achieved, for $P_{max} = 40$ dBm, by the same resource allocation schemes of Fig. 6. Similar observations to those for Fig. 6 can be made, with the notable difference that the EE obtained with uniform power allocation (i.e. no optimization of $\boldsymbol{Q}$) and RHS optimization is significantly worse than the corresponding capacity that is shown in Fig. 6. This is explained because the uniform power allocation is a strategy that employs all the available power P_{max}, and in Fig. 7 it was set $P_{max} = 40$ dBm, which is a rather high power value. Thus, adopting uniform power allocation with $P_{max} = 40$ dBm is much more detrimental for the EE shown in Fig. 7, than for the capacity shown in Fig. 6. Moreover, it is also seen that the EE increases with N, even though at a slower rate than the capacity. This happens because, as N increases, both the capacity and the hardware power consumption increase. Eventually, for larger values of N, the EE will start decreasing with N, since the numerator increases logarithmically while the denominator linearly with N.

7 Conclusions

A MIMO communication link has been considered, in which an RHS is deployed in the near field of the transmit antenna array. Two optimization algorithms have been proposed to optimize the system EE and the capacity, by allocating the transmit covariance matrix and the RHS reflection matrix. The first algorithm uses the framework of sequential fractional programming, while the second algorithm employs a search in a standard-compliant codebook for the optimization of the transmit covariance matrix, and the use of sequential optimization for RHS optimization. The two algorithms achieve different

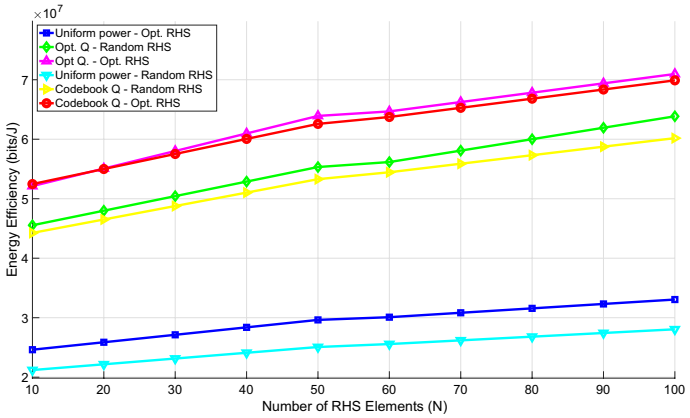

Fig. 7 EE versus number of reflecting elements of the RHS for different resource allocation policies

performance-complexity trade-offs with the codebook one being less complex, and suffering a limited penalty compared to the more sophisticated one that employs sequential fractional programming. Numerical results confirm the merits of the proposed algorithm in improving the performance of the system in terms of EE and capacity, with respect to a scenario in which the optimization is not performed.

Appendix 1: Sequential optimization

The sequential optimization framework is an iterative method that tackles non-convex problems by solving a sequence of surrogate problems. If the surrogate problems fulfill specific assumptions, then their solutions form a sequence of feasible points for the original problem, monotonically increasing the objective function, and eventually converging to a point fulfilling the Karush–Kuhn–Tucker (KKT) optimality conditions of the original problem. To elaborate let $\mathcal{P}$ be the optimization problem

$$\mathcal{P} \ : \min_{\boldsymbol{x}} g_1(\boldsymbol{x}) \tag{A1a}$$

$$g_\ell(\boldsymbol{x}) \leq 0 \ , \forall \ell = 2, \ldots, L \tag{A1b}$$

In order to tackle $\mathcal{P}$, the sequential optimization framework requires finding a sequence of differentiable convex functions $\{\bar{g}_{i,\ell}(\boldsymbol{x})\}_i$, and a sequence of feasible points $\bar{\boldsymbol{x}}_i$, such that, for any $\ell = 1, \ldots, L$, it holds

$$\bar{g}_{i,\ell}(\boldsymbol{x}) \leq g_\ell(\boldsymbol{x}) \ , \ \forall \boldsymbol{x} \tag{A2}$$

$$\bar{g}_{i,\ell}(\bar{\boldsymbol{x}}_i) = g_\ell(\bar{\boldsymbol{x}}_i) \tag{A3}$$

$$\nabla_{\boldsymbol{x}} \bar{g}_{i,\ell}(\bar{\boldsymbol{x}}_i) = \nabla_{\boldsymbol{x}} g_\ell(\bar{\boldsymbol{x}}_i) \tag{A4}$$

Then, the following result holds [46].

Proposition 3

Consider the sequence of problems $\mathcal{P}_i$ defined as

$$\mathcal{P}_i \ : \min_{\boldsymbol{x}} \bar{g}_{i,1}(\boldsymbol{x}) \tag{A5a}$$

$$\bar{g}_{i,\ell}(\boldsymbol{x}) \leq 0 \ , \forall \ell = 2, \ldots, L \tag{A5b}$$

and denote by $\boldsymbol{x}_i^\star$ its solution. Then, if, for all i, $\bar{\boldsymbol{x}}_{i+1} = \boldsymbol{x}_i^\star$, then the sequence $\{g(\boldsymbol{x}_i^\star)\}_i$ is monotonically increasing and converges to a point fulfilling the KKT conditions of Problem $\mathcal{P}$.

Acknowledgements
Not applicable.

Author Contributions
A. T. developed the codebook approach and contributed to the simulation. R. F. developed the fractional programming approach and contributed to the simulation. A. Z. contributed to the development of the algorithms and writing of the manuscript. G. T. contributed to the development of the algorithms and writing of the manuscript. G. A. contributed to the writing of the manuscript.

Funding
The work of A. I. Tunali has received funding from the European Commission through the project HE-DN-INTEGRATE, grant agreement number 101072924. The work of R. Fotock has received funding from the Project "GARDEN", funded by EU in NextGeneration EU plan, Mission 4, Component 1, CUP H53D23000480001, through the Italian "Bando Prin 2022 - D.D. 104 del 02-02-2022" by MUR. The work of A. Zappone has been funded by the European Union - NextGenerationEU under the project NRRP RESTART, RESearch and innovation on future Telecommunications systems and networks, to make Italy more smART PE_00000001 - Cascade Call SPARKS project, with CUP D43C22003080001. The work of G. Alfano has been funded by the European Union - NextGenerationEU under the project NRRP RESTART, RESearch and innovation on future Telecommunications systems and networks, to make Italy more smART PE_00000001 - Cascade Call SMART project, with CUP E63C22002040007.

Data Availability
The datasets generated and/or analyzed during the current study are available from the first and second authors on reasonable request.

Declarations

Ethics approval and consent to participate
Not applicable.

Consent for publication
Not applicable.

Conflict of interest
The authors declare that they have no conflict of interest.**Received: 30 March 2025 Accepted: 18 June 2025**
Published online: 20 July 2025

References

1. M. Di Renzo, M. Debbah, D.-T. Phan-Huy, A. Zappone et al., Smart radio environments empowered by reconfigurable AI meta-surfaces: an idea whose time has come. EURASIP J. Wirel. Commun. Netw. **129** (2019)
2. Q. Wu, R. Zhang, Towards smart and reconfigurable environment: intelligent reflecting surface aided wireless network. IEEE Commun. Mag. (2019)
3. C. Huang, G.C. Alexandropoulos, C. Yuen, M. Debbah, Indoor signal focusing with deep learning designed reconfigurable intelligent surfaces. In: 2019 IEEE 20th International Workshop on Signal Processing Advances in Wireless Communications (SPAWC), pp. 1–5 (2019). IEEE
4. Y. Yuan, Y. Huang, X. Su, B. Duan, N. Hu, M. Di Renzo, Reconfigurable intelligent surface (RIS) system level simulations for industry standards. arxiv: 2409.13405 (2024)
5. Huawei Technologies: Green 5G building a sustainable world. https://www.huawei.com/en/public-policy/green-5g-building-a-sustainable-world (2020)
6. R. Long, Y.C. Liang, Y. Pei, E.G. Larsson, Active reconfigurable intelligent surface-aided wireless communications. IEEE Trans. Wirel. Commun. **20**(8), 4962–4975 (2021)
7. Z. Zhang et al., Active RIS vs. passive RIS: Which will prevail in 6G? IEEE Trans. Commun. **71**(3), 1707–1725 (2023)

8. R.K. Fotock, A. Zappone, M. Di Renzo, Energy efficiency optimization in RIS-aided wireless networks: active versus nearly-passive RIS with global reflection constraints. IEEE Trans. Commun. **72**(1), 257–272 (2023)
9. C. Huang, A. Zappone, G.C. Alexandropoulos, M. Debbah, C. Yuen, Reconfigurable intelligent surfaces for energy efficiency in wireless communication. IEEE Trans. Wirel. Commun. **18**(8), 4157–4170 (2019)
10. Q. Wu, R. Zhang, Intelligent reflecting surface enhanced wireless network: joint active and passive beamforming design. IEEE Trans. Wirel. Commun. **18**(11), 5394–5409 (2019)
11. Y. Chen, Y. Wang, Z. Wang, P. Zhang, Robust beamforming for active reconfigurable intelligent omni-surface in vehicular communications. IEEE J. Sel. Areas Commun. **40**(10), 3086–3103 (2022)
12. Q. Zhu, M. Li, R. Liu, Y. Liu, Q. Liu, Joint beamforming designs for active reconfigurable intelligent surface: a sub-connected array architecture. IEEE Trans. Commun. **70**(11), 7628–7643 (2022)
13. K. Liu, Z. Zhang, L. Dai, S. Xu, F. Yang, Active reconfigurable intelligent surface: Fully-connected or sub-connected? IEEE Commun. Lett. **26**(1), 167–171 (2022)
14. Y. Ma, M. Li, Y. Liu, Q. Wu, Q. Liu, Active reconfigurable intelligent surface for energy efficiency in MU-MISO systems. IEEE Trans. Veh. Technol. **72**(3), 4103–4107 (2023)
15. Q. Peng, Q. Wu, G. Chen, R. Liu, S. Ma, W. Chen, Hybrid active-passive IRS assisted energy-efficient wireless communication. IEEE Commun. Lett. **27**(8), 2202–2206 (2023)
16. Y. Wang et al., Secure satellite transmission with active reconfigurable intelligent surface. IEEE Commun. Lett. **26**(12), 3029–3033 (2022)
17. Y. Zhang, Y. Lu, R. Zhang, B. Ai, D. Niyato, Deep reinforcement learning for secrecy energy efficiency maximization in RIS-assisted networks. IEEE Trans. Veh. Technol. **72**(9), 12413–12418 (2023). https://doi.org/10.1109/TVT.2023.3269805
18. Y. Lu, Secrecy energy efficiency in RIS-assisted networks. IEEE Trans. Veh. Technol. **72**(9), 12419–12424 (2023). https://doi.org/10.1109/TVT.2023.3269905
19. W. Hao, J. Li, G. Sun, C. Huang, M. Zeng, O.A. Dobre, C. Yuen, Max-min security energy efficiency optimization for RIS-aided cell-free networks. In: 2023 IEEE International Communications Conference (2023)
20. R. Deng, B. Di, H. Zhang, D. Niyato, Z. Han, H.V. Poor, L. Song, Reconfigurable holographic surfaces for future wireless communications. IEEE Wirel. Commun. **28**(6), 126–131 (2021)
21. T. Gong et al., Holographic MIMO communications: theoretical foundations, enabling technologies, and future directions. IEEE Commun. Surv. Tutor. **26**(1), 196–257 (2023)
22. S. Zeng, H. Zhang, B. Di, H. Qin, X. Su, L. Song, Reconfigurable refractive surfaces: an energy-efficient way to holographic MIMO. IEEE Commun. Lett. **26**(10), 2490–2494 (2022)
23. L. You et al., Energy efficiency maximization of massive MIMO communications with dynamic metasurface antennas. IEEE Trans. Wireless Commun. **22**(1), 393–407 (2022)
24. S. Guo, J. Ye, K. Qu, S. Dang, Green holographic MIMO communications with a few transmit radio frequency chains. IEEE Trans. Green Commun. Netw. **8**(1), 90–102 (2023)
25. L. Wei, C. Huang, G.C. Alexandropoulos, E. Wei, Z. Zhang, M. Debbah, C. Yuen, Multi-user holographic MIMO surfaces: channel modeling and spectral efficiency analysis. IEEE J. Sel. Top. Signal Process. **16**(5), 1112–1124 (2022)
26. B. Di, H. Zhang, Z. Han, R. Zhang, L. Song, Reconfigurable holographic surface: a new paradigm for ultra-massive MIMO. IEEE Trans. Cogn. Commun. Netw. (2025)
27. Q. Li, M. El-Hajjar, Y. Sun, I. Hemadeh, A. Shojaeifard, L. Hanzo, Energy-efficient reconfigurable holographic surfaces operating in the presence of realistic hardware impairments. IEEE Trans. Commun. **72**(8), 5226–5238 (2024)
28. T. Gong, L. Wei, C. Huang, Z. Yang, J. He, M. Debbah, C. Yuen, Holographic MIMO communications with arbitrary surface placements: near-field IoS channel model and capacity limit. IEEE J. Sel. Areas Commun. **42**(6), 1549–1566 (2024)
29. J. An, C. Xu, D.W.K. Ng, G.C. Alexandropoulos, C. Huang, C. Yuen, L. Hanzo, Stacked intelligent metasurfaces for efficient holographic MIMO communications in 6G. IEEE J. Sel. Areas Commun. **41**(8), 2380–2396 (2023)
30. Z. Wan, Z. Gao, F. Gao, M. Di Renzo, M.-S. Alouini, Terahertz massive MIMO with holographic reconfigurable intelligent surfaces. IEEE Trans. Commun. **69**(7), 4732–4749 (2021)
31. A.T. Joy, A. Tishchenko, H. Taghvaee, P. Botham, F. Burton, M. Khalily, R. Tafazolli, From reconfigurable intelligent surfaces to holographic MIMO surfaces and back. In: 2024 18th European Conference on Antennas and Propagation (EuCAP), pp. 1–5 (2024). IEEE
32. M. Qian, L. You, X.-G. Xia, X. Gao, On the spectral efficiency of multi-user holographic MIMO uplink transmission. IEEE Trans. Wirel. Commun. **23**(10), 1521–15434 (2024)
33. A. Zappone, B. Matthiesen, A. Dekorsy, Energy efficiency of holographic transceivers based on RIS. In: GLOBECOM 2022-2022 IEEE Global Communications Conference (2022)
34. S. Zeng, H. Zhang, B. Di, L. Song, Reconfigurable refractive surface-enabled multi-user holographic MIMO communications. IEEE Trans. Wirel. Commun. **23**(5), 4845–4860 (2023)
35. G. Interdonato, F. Di Murro, C. D'Andrea, G. Di Gennaro, S. Buzzi, Approaching massive mimo performance with reconfigurable intelligent surfaces: we do not need many antennas. IEEE Trans. Commun. (2024)
36. A. Mishra, Y. Mao, C. D'Andrea, S. Buzzi, B. Clerckx, Tansmitter side beyond-diagonal reconfigurable intelligent surface for massive MIMO networks. IEEE Wirel. Commun. Lett. **13**(2), 352–356 (2024)
37. Y. Song, J. Jalali, F. Lemic, N. Devroye, J. Famaey, Miniature UAV empowered reconfigurable energy harvesting holographic surfaces in THz cooperative networks. arxiv: 2411.18791 (2025)
38. J. Jalali, M. Darabi, R.C. de Lamare: shape adaptive reconfigurable holographic surfaces. arxiv: 2503.21542 (2025)
39. A. Zappone, M. Di Renzo, F. Shams, X. Qian, M. Debbah, Overhead-aware design of reconfigurable intelligent surfaces in smart radio environments. IEEE Trans. Wirel. Commun. **20**(1), 126–141 (2021)
40. L. You, J. Xiong, D.W.K. Ng, C. Yuen, W. Wnag, X. Gao, Energy efficiency and spectral efficiency tradeoff in RIS-aided multiuser MIMO uplink transmission. IEEE Trans. Signal Process. 1407–1421 (2021)
41. V. Sharma et al., A pricing-based approach for energy-efficiency maximization in RIS-aided multi-user MIMO SWIPT-enabled wireless networks. IEEE Access **10**, 29132–29148 (2022)

42. M. Soleymani, I. Santamaria, E.A. Jorswieck, R. Schober, L. Hanzo, Optimization of the downlink spectral- and energy-efficiency of RIS-aided multi-user URLLC MIMO systems. IEEE Trans. Commun. (2024)
43. V. Degli-Esposti, E.M. Vitucci, M. Di Renzo, S. Tretyakov, Reradiation and scattering from a reconfigurable intelligent surface: a general macroscopic model. IEEE Trans. Antenna Propag. **70**(10), 8691–8706 (2022)
44. C. Feng, H. Lu, Y. Zeng, T. Li, S. Jin, R. Zhang, Near-field modelling and performance analysis for extremely large-scale IRS communications. IEEE Trans. Wirel. Commun. **23**(5), 4976–4989 (2024)
45. R.A. Horn, C.R. Johnson, *Matrix Analysis* (Cambridge University Press, Cambridge, 1985)
46. B.R. Marks, G.P. Wright, A general inner approximation algorithm for non-convex mathematical programs. Oper. Res. **26**(4), 681–683 (1978)
47. A. Zappone, E.A. Jorswieck, Energy efficiency in wireless networks via fractional programming theory. Found. Trends® Commun. Inf. Theory **11**(3–4), 185–396 (2015)
48. Ericsson: Advanced CSI codebook structure. TSG-RAN WG1 #87 RI-161266, Ericsson (2016)
49. 3GPP: NR; Physical layer procedures for data. Technical Specification (TS) 38.214, 3rd Generation Partnership Project (3GPP) (January 2024). Version 18.1.0. https://portal.3gpp.org/desktopmodules/Specifications
50. Intel: On NR Type I codebook. Tsg ran wg1 #88 r1-1702205, Intel (2017)
51. A. Ben-Tal, A. Nemirovski, Lectures on modern convex optimization. MPS-SIAM (2001)

Publisher's Note

Springer Nature remains neutral with regard to jurisdictional claims in published maps and institutional affiliations.